Polarization-modulation-based orientation metrology of optically levitated rotating birefringent particles

Kai Zeng, Yulie Wu,* Xuezhong Wu, and Dingbang Xiao†
College of Intelligence Science and Technology, National University of Defense Technology, Changsha 410073, China

(Received 2 September 2023; revised 16 November 2023; accepted 11 January 2024; published 12 February 2024)

The ultrafast rotation of optically levitated particles has propelled advancements in sensing and precision measurement, while its orientation remains largely unexplored for the spherical shape. Here, we proposed an orientation measurement method for the birefringent rotating particles, which extracts both the azimuthal and polar angles of the optical axis from the polarization of the transmitted laser. A bulk birefringent crystal with a known orientation is measured by this method to verify its effectiveness, and then the orientation of vaterite particles is extracted from the rotational signal. This method paves the way to investigate the orientational dynamics and gyroscope application.

DOI: 10.1103/PhysRevResearch.6.013160

I. INTRODUCTION

The optically levitated particles have significantly advanced measurement technologies and fundamental physics [1–5]. Center-of-mass (COM) motion of the levitated particles is employed for sensing weak force [6,7] and acceleration [8,9], while rotation is utilized to measure torque [10,11], as well as other physical quantities associated with rotational drag torque [12–14]. The levitated particle can be induced to rotate at exceptionally high frequencies in the GHz range [15–17], and the ultrafast rotating particles in a vacuum environment serves as a research platform for studying vacuum friction [18,19], as well as Casimir force and torque [20,21].

Recently, the orientation of optically levitated particles shows great potential in quantum science, coupling dynamics and orientation-based sensing. The optically levitated particles show pronounced interference effects in their orientation, which makes orientational quantum interference attractive for testing and exploiting quantum physics with massive objects [22–24]. The orientation measurement of the particle is one of technological obstacles to observe these orientational quantum phenomenons. Additionally, the orientation-related precession of rotating particles is observed and can be used for torque sensing with the sensitivities capable of resolving single-electron and nuclear spins [25–27]. When the birefringent particle is trapped by linearly polarized laser, the orientation of the particle optical axis shows great coupling with the COM motion, and the ultrahigh mechanical quality factor is obtained by parametrically driving [28,29]. However, despite the focus on particle orientation in these studies, an effective orientation measurement method is currently unavailable. Therefore, only the frequency information of these dynamics is presented. For particles made of birefringent crystal material, the orientation of the optical axis can cause a change in the polarization of the transmitted laser, offering a potential orientation measurement technique [30,31].

Here, we proposed a method to measure the orientation of the optically levitated birefringent particles. This method is first tested in a bulk birefringent crystal, as its optical axis can be distinguished and controlled easily. Then, the optical axis of vaterite particles is measured, allowing for the determination of both azimuthal and polar angle. Meanwhile, a supplemental laser is introduced in the transverse direction to simultaneously monitor the orientation.

II. MEASUREMENT PRINCIPLE

As shown in Fig. 1(a), the orientation of a levitated rotating vaterite particle is challenging to be determined for its spherical shape. In contrast to its symmetric shape, the vaterite particle exhibits anisotropic optical properties. The orientation of the optical axis is defined as shown in Fig. 1(b), where the azimuthal angle is α and polar angle is θ. The optical axis is an intrinsic direction of the birefringent materials, which can be used to determine the orientation of the particle.

As shown in Figs. 1(c)–1(d), assuming a circularly polarized laser incident perpendicularly onto a positive uniaxial birefringent crystal (the refractive index $n_o < n_e$) along the positive z-axis direction, the polarization of the transmitted laser experiences alterations influenced by parameters such as crystal thickness, refractive index, and optical axis orientation. The incident laser can be expressed by two linearly polarized parts in the crystal, namely ordinary laser (OL) and extraordinary laser (EL). The propagation direction of OL and EL coincides but the polarization direction is perpendicular. The velocity v_o of OL is constant along any direction in the crystal, while the velocity v_θ of EL varies with the polar

*ylwu@nudt.edu.cn
†dingbangxiao@nudt.edu.cn

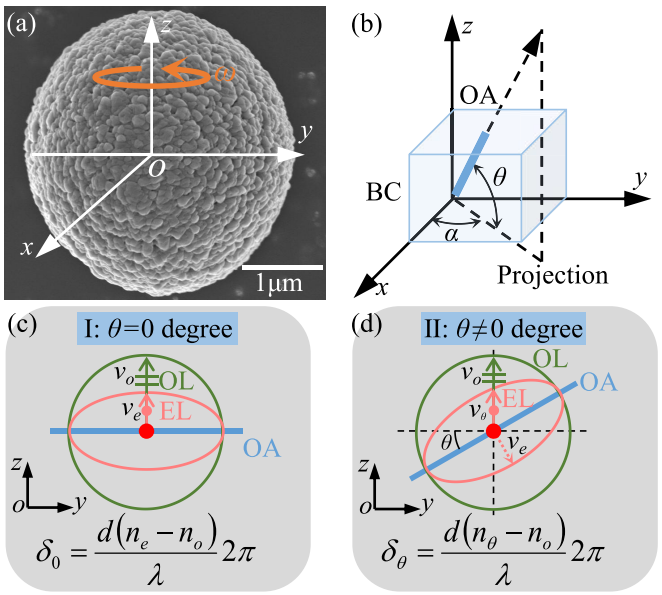

FIG. 1. Orientation definition and measurement principle. (a) Scanning electron microscope image of a vaterite particle. (b) Orientation definition of the optical axis. OA: optical axis; BC: birefringent crystal. (c)–(d) Transmitting characteristics of ordinary laser (OL) and extraordinary laser (EL) in BC for (c) $\theta = 0$ and (d) $\theta \neq 0$, and the azimuths are both 0. The green circle indicates uniform velocity of OL in all directions, while the pink ellipse illustrates the elliptical distribution of velocity for EL.

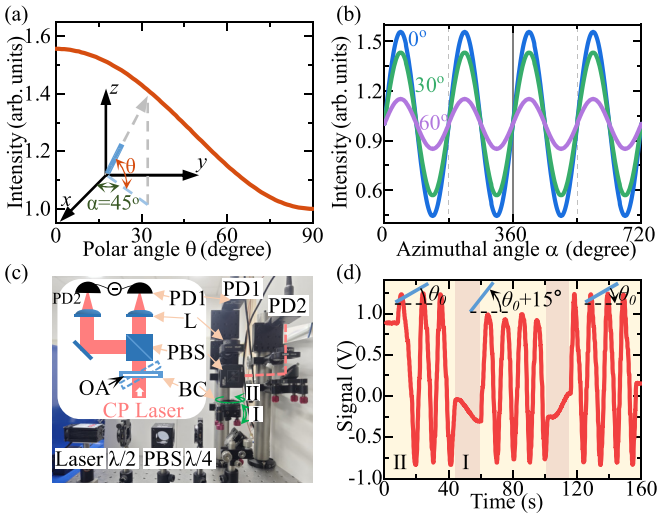

FIG. 2. Simulated results and experimental verification. (a) Simulated results of laser intensity versus polar angle θ. The azimuthal angle $\alpha = 45°$, electric field amplitude $E_0 = 1$. (b) Simulated intensity when the crystal rotate. The rotating angular frequency is $\omega = 5 \times 2\pi$. (c) Experimental setup for a circularly polarized (CP) laser transmitting the birefringent crystal (BC). Labels denote the half wave plate ($\lambda/2$), polarizing beam splitter (PBS), quarter wave plate ($\lambda/4$), lens (L), photodetector (PD). Inset shows the birefringence effect, and the double image of lines can be seen through the birefringent crystal. The signals from two detectors are differentiated to improve the signal-to-noise ratio. (d) The measured voltage signal under different manipulation. I represents the tilt (θ) of the crystal, and II represents the rotation (α). The same color represents the same manipulation.

angle θ. Generally, v_θ changes between v_e and v_o, and obeys an elliptical distribution (pink ellipse) as shown in Fig. 1(d). When the velocity of OL and EL differ (corresponding to the different refractive index $n = c/v$, where c is the light velocity in vacuum), a phase delay δ_θ occurs, which affects the polarization of the laser that transmitted through the birefringent crystal.

The phase delay is derived as $\delta_\theta = 2\pi d(n_\theta - n_o)/\lambda$, where d is the thickness of crystal, λ is the wavelength of laser. In this case, the electric field of the transmitted laser can be expressed as

$$\begin{cases} E_{\mathrm{OL}} = E_{\mathrm{OL0}} \cos(\omega_0 t) \\ E_{\mathrm{EL}} = E_{\mathrm{EL0}} \cos(\omega_0 t + \pi/2 + \delta_e), \end{cases} \tag{1}$$

where $E_{\mathrm{OL0}} = E_{\mathrm{EL0}} = E_0$, and the n_θ in the δ_θ can be calculated according to the elliptical distribution in Fig. 1(d)

$$n_\theta = \sqrt{n_o^2 \sin^2\theta + n_e^2 \cos^2\theta}. \tag{2}$$

The transmitted laser is usually elliptically polarized, and the ellipticity of the polarization ellipse is determined by the phase delay δ_θ. Because δ_θ is related to the polar angle θ, the polar angle θ hence can be obtained by measuring the ellipticity. Besides, the azimuth of the polarization ellipse would follow the rotation of the optical axis. Therefore, the azimuth of the optical axis can also be obtained by measuring the polarization ellipse.

A polarizer is used in the detection system [the PBS in Fig. 2(c) for instance] to detect the polarization information. Assuming the transmission direction of the polarizer lies in the x axis, the angle between the transmission direction and the optical axis is also α. Hence, the transmitted laser intensity I can be expressed as [30]

$$I = E_0^2[1 + \sin(2\alpha)\sin\delta_\theta]. \tag{3}$$

The detected laser intensity can also be written as $I = 2P/\pi/a^2$ [32], where P is the detected laser power, a is the radius of laser. The voltage from PD is expressed as $V = PG$, where G is the conversion gain of the detector. Substituting Eqs. (1)–(3) into this equation, the relation between the voltage and the azimuthal angle α and polar angle θ is

$$V = kP_0G\left(1 + \sin(2\alpha)\sin\left[\frac{d\left(\sqrt{n_o^2\sin^2\theta + n_e^2\cos^2\theta} - n_o\right)}{\lambda} 2\pi\right]\right), \tag{4}$$

where $P_0 \propto E_0^2$ is the inputted laser power, k is the attenuation coefficient.

III. EXPERIMENTAL VERIFICATION

Figure 2(a) illustrates the simulated laser intensity as a function of the polar angle θ while the azimuthal angle α is held constant. As the polar angle increase, the refractive index n_θ decreases, resulting in a decrease in phase delay. This reduction makes the transmitted laser approached circular polarization, and the laser intensity shows the rule in Fig. 2(a).

On the contrary, when the polar angle θ remains constant, the relationship between intensity and the rotation angle is shown in Fig. 2(b). As the crystal rotates with respect to the laser propagation direction with a frequency of $\omega = 5 \times 2\pi$ rad/s, the intensity changes periodically with frequency 2ω due to the repetition of optical axis every 180°. This phenomenon also explains the observed rotational signal frequency of the levitated particle being twice the spin frequency [25,33]. By analyzing the variation, the azimuthal angle α can be read out. For example, when the intensity is at the middle value, the azimuth α is 0°. The azimuth changes by 180° for each cycle of intensity change, and it changes by 90° when the intensity increase from the minimum to the maximum value. Meanwhile, the polar angle of the optical axis can also be read out by examining the amplitude of the rotational signal as shown in the Fig. 2(b).

Furthermore, these results are experimentally validated, and the setup is shown in the Fig. 2(c). The laser power is controlled using the $\lambda/2$ and the PBS, and the circularly polarized laser is incident on the birefringent crystal after passing the $\lambda/4$. The birefringent crystal is mounted on a multiaxis frame, which allows for tilting and rotation. After the laser passing through the crystal, a PBS is used as the polarizer, and the measured results are shown in Fig. 2(d). When the birefringent crystal rotates with respect to the laser propagation direction, the measured voltage signal changes periodically, with a variation frequency that is twice the rotation frequency. The initial angle θ_0 is about 37°, which is related to the optical axis orientation and shape of the birefringent crystal. When the angle θ increased by 15°, the measured signal amplitude decreased by 16.5%, and the simulated result is 10.6%. The excessive reduction comes from the defects in the actual birefringent crystal, such as cracks and impurities. Upon ceasing tilting and resuming rotation, the amplitude of the rotational signal decreases, indicating a change in the ellipticity of the polarization ellipse due to the tilting. Besides, the asymmetrical changes result from the imperfect circular polarization of the incident laser and the manual manipulation.

IV. ORIENTATION MEASUREMENT

The experimental setup for particle orientation measurement is presented in Fig. 3(a). A vertically oriented trapping laser is employed to trap particles within the vacuum chamber, and the transmitted laser is collected by the detection system to acquire motion signals. In addition, a weakly focused horizontal laser (transverse laser) is introduced to enhance the validation of orientation measurements. The birefringent

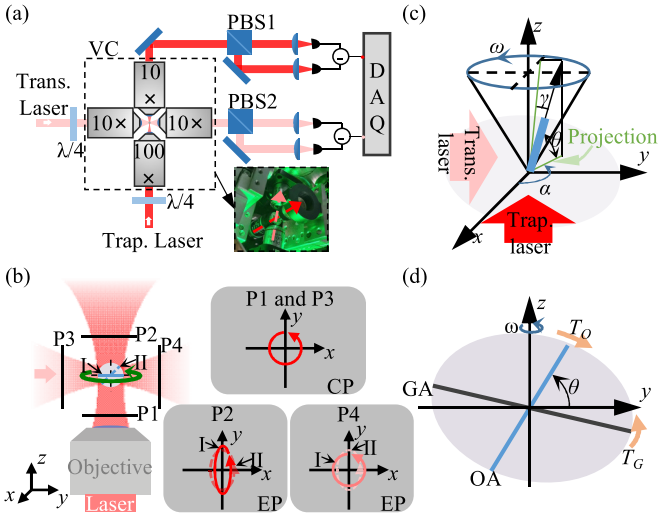

FIG. 3. Experimental setup and orientation measurement method of the vaterite particles. (a) Diagram of the experimental setup. The trapping laser (1064 nm, 20 mW) is focused from the bottom to the vacuum chamber (VC) using a high numerical aperture (NA = 1.25) objective. The transverse laser is horizontally oriented, featuring a weaker focus (NA = 0.25) and low power (0.5 mW). Inset shows the focusing and collecting objective of the two lasers. (b) Sketch map of the laser polarization before and after the particles. $P1$–$P4$ represent different planes. Case I: optical axis in xoy plane. (c) Illustration of the polar angle of the optical axis respect to the trapping laser (θ) and transverse laser polarization plane (γ). (d) The deviation of the optical axis from the trapping laser polarization plane under the centrifugal torque T_G. GA and OA represents the geometrical long axis and optical axis respectively. T_O represents the optical alignment torque.

particles utilized in the experiments are vaterite particles with diameter 3.58 ± 0.2 μm.

As shown in Fig. 3(b), both the trapping laser and the transverse laser in $P1$ and $P3$ are circularly polarized. However, the transmitted laser exhibits elliptical polarization due to the phase delay. As analyzed in Eq. (2), when the optical axis aligns with the polarization plane (case I) of trapping laser, the delay reaches the maximum value, and the ellipticity of the polarization ellipse in $P2$ is also maximum. For the scenario that the optical axis deviates from the polarization plane (case II), the ellipticity of the transmitted laser decreases. On the contrary, since the polarization plane of the transverse laser is perpendicular to the optical axis in case I, the polarization in $P4$ remains circularly polarized (assuming the azimuth $\alpha = 90°$). In case II, the laser becomes elliptically polarized, and the ellipticity increase with the polar angle θ. As shown in Fig. 2(c), using the detection method, the amplitude of the rotational signal would increase with increased ellipticity. Therefore, from case I to case II, the measured amplitude decreases in the trapping laser direction and increases in the transverse laser direction.

The polar and azimuthal angle of the optical axis is sketched in Fig. 3(c). The polar angle θ remains constant with the spin rotation ω of the particle (along z axis), while the polar angle γ varies as

$$\cos\gamma = \sqrt{\sin^2(\omega t) + \cos^2(\omega t)\sin^2\theta}. \tag{5}$$

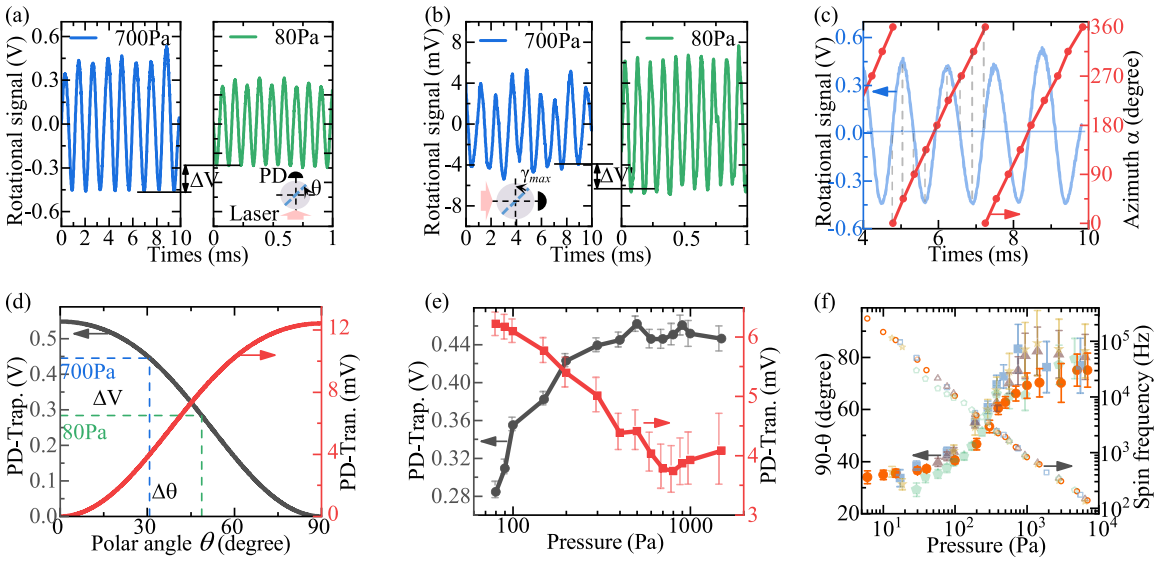

FIG. 4. Measured orientation results of optically levitated particles. (a)–(b) Rotational signal from (a) trapping laser and (b) transverse laser under different pressure. The rotational frequencies at 700 Pa and 80 Pa are 791 Hz and 9925 Hz, respectively. PD represents photodetector. (c) Azimuth α of the optical axis. The dashed line indicates the converting from the rotational signal to azimuth. (d) Calculated amplitude of rotational signal versus polar angle θ. The value is calibrated when $\theta = 0^\circ$, and the polar angle can be read out from the measured rotational signal. (e) Measured amplitude of rotational signal under different pressure. Error bar comes from the standard deviation. (f) Spin frequency and polar angle of five particles versus pressure. The polar angle is expressed as 90°-θ for visualization purposes.

The angle γ still decreases with the increase of θ. Besides, the intensity of the transmitted transverse laser follows Eq. (3), and the azimuth changes with angular frequency ω. Although γ changes with rotation, the measured rotational signal shows periodic changes, and the amplitude monotonically increases with polar angle θ. Therefore, the proposed method can still be employed to obtain the polar angle γ, which reaches its maximum value $\gamma_{\max}$ ($\gamma_{\max} + \theta = \pi/2$) when the azimuth $\alpha = k\pi$, k is integer.

As shown in Fig. 3(d), due to the fact that the particle is not a perfect sphere, the geometrical long axis (GA) would produce centrifugal torque T_G that tilts the GA to the rotation plane (xoy plane) [31]. In other words, T_G drives the heavier end to the rotation plane. Meanwhile, there is a torque T_O that aligns the optical axis with the polarization plane (also xoy plane) [27,34]. Hence, the two torques T_G and T_O balance each other. Since T_G increases with the spin frequency, the polar angle θ can be manipulated by controlling the particle spin frequency.

Based on the optical axis manipulating method, the spin frequency of the particle is increased by reducing the environmental pressure, which results in the tilting of the optical axis away from the polarization plane of the trapping laser. During the acceleration of the rotation, the rotational signal is measured as depicted in Figs. 4(a)–4(b). The rotational signal from the trapping laser exhibits reduced amplitude under the lower pressure (corresponding to a faster spin frequency), whereas the amplitude increases for the transverse laser. This variation indicates that the centrifugal torque tilts the optical axis, and the polar angle θ increased. Meanwhile, the periodic variation of the rotational signal versus time correlates with the long axis of the polarization ellipse, which can be used to determine the azimuth of the optical axis. According to Eq. (3), the azimuth α is obtained as shown in Fig. 4(c).

The polar angles are extracted from the measured rotational signal as shown in Fig. 4(d). The amplitude variation of rotational signal from trapping laser and transverse laser are calculated from Eq. (4). Since the centrifugal torque is negligible at low spin frequency (usually 30–50 Hz at atmosphere), the optical axis will align with the polarization plane of trapping laser due to the torque T_O. In this case, the initial polar angle θ is considered to be approximately zero, and the coefficient k is calibrated. Hence, the measured ΔV can be converted to the changes of the polar angle. As shown in Fig. 4(e), the amplitude of rotational signal in the trapping laser direction decreases as the pressure decreases, indicating a deviation of the optical axis from the polarization plane. This phenomenon is simultaneously monitored by the transverse laser, and the amplitude shows a gradual increase. Since the polarization planes of the trapping laser and the transverse laser are perpendicular, any deviation of the optical axis from one plane necessitates its approach towards the other.

Figure 4(f) shows converted polar angle of five particles as function of the pressure. The values of different particles may vary for the material and shape uniformity, but the overall pattern of changes is consistent. The spin-frequency-related centrifugal torque leads to the deviations in optical axis, which means the angle 90°-θ decreases. It is worth mentioning that the decrease rate of the angle slows down after a sharp decline between 100–1000 Pa. The rationale behind this is that the centrifugal torque has tilted the geometrical long axis to the proximity of the rotation plane with high spin frequency. As the mean value stabilizes, there is a reduction in the fluctuation (standard deviation) of the angle, which corresponds to the gyroscopic orientation stabilization [25]. However, as the pressure decreases further, the fluctuation would increase. The increase is the result of the thermal Brownian motion for the cooling from the residual gas becomes ineffective in vacuum

[35,36], and the gyroscopic stabilization can not suppress the thermal effect at further low pressure.

V. CONCLUSION

In the realm of levitated optomechanical systems, there has been extensive research on both the center-of-mass motion and particle rotation. To further explore the gyroscopic dynamics in optically levitated particles, we proposed an orientation measurement method for optically levitated vaterite particles based on the polarization modulation. It is verified by a bulk birefringent crystal, and the particle orientation is obtained from its rotational signal. This approach not only aids in investigating particle dynamic characteristics such as precession, nutation, and gyroscopic stabilization [37,38] but also lays the groundwork for orientational quantum interference [22–24] and potential gyroscopes application [39].

ACKNOWLEDGMENT

This project was supported by the National Natural Science Foundation of China (Grant No. 51975579).

[1] C. Gonzalez-Ballestero, M. Aspelmeyer, L. Novotny, R. Quidant, and O. Romero-Isart, Levitodynamics: Levitation and control of microscopic objects in vacuum, Science **374**, eabg3027 (2021).

[2] J. Millen, T. S. Monteiro, R. Pettit, and A. N. Vamivakas, Optomechanics with levitated particles, Rep. Prog. Phys. **83**, 026401 (2020).

[3] U. Delic, M. Reisenbauer, K. Dare, D. Grass, V. Vuletic, N. Kiesel, and M. Aspelmeyer, Cooling of a levitated nanoparticle to the motional quantum ground state, Science **367**, 892 (2020).

[4] F. Tebbenjohanns, M. L. Mattana, M. Rossi, M. Frimmer, and L. Novotny, Quantum control of a nanoparticle optically levitated in cryogenic free space, Nature (London) **595**, 378 (2021).

[5] L. Magrini, P. Rosenzweig, C. Bach, A. Deutschmann-Olek, S. G. Hofer, S. Hong, N. Kiesel, A. Kugi, and M. Aspelmeyer, Real-time optimal quantum control of mechanical motion at room temperature, Nature (London) **595**, 373 (2021).

[6] S. Zhu, Z. Fu, X. Gao, C. Li, Z. Chen, Y. Wang, X. Chen, and H. Hu, Nanoscale electric field sensing using a levitated nanoresonator with net charge, Photon. Res. **11**, 279 (2023).

[7] G. Ranjit, M. Cunningham, K. Casey, and A. A. Geraci, Zeptonewton force sensing with nanospheres in an optical lattice, Phys. Rev. A **93**, 053801 (2016).

[8] D. S. Bykov, O. A. Schmidt, T. G. Euser, and P. Russell, Flying particle sensors in hollow-core photonic crystal fibre, Nature Photon. **9**, 461 (2015).

[9] F. Monteiro, W. Li, G. Afek, C. L. Li, M. Mossman, D. C. Moore, Force and acceleration sensing with optically levitated nanogram masses at microkelvin temperatures, Phys. Rev. A **101**, 053835 (2020).

[10] T. A. Nieminen, N. R. Heckenberg, and H. Rubinsztein-dunlop, Optical measurement of microscopic torques, J. Mod. Opt. **48**, 405 (2001).

[11] J. Ahn, Z. Xu, J. Bang, P. Ju, and T. Li, Ultrasensitive torque detection with an optically levitated nanorotor, Nature Nanotechnol. **15**, 89 (2020).

[12] C. P. Blakemore, D. Martin, A. Fieguth, A. Kawasaki, N. Priel, A. D. Rider, and G. Gratta, Absolute pressure and gas species identification with an optically levitated rotor, J. Vac. Sci. Technol. B **38**, 024201 (2020).

[13] S. Kuhn, B. A. Stickler, A. Kosloff, F. Patolsky, K. Hornberger, M. Arndt, and J. Millen, Optically driven ultra-stable nanomechanical rotor, Nature Commun. **8**, 1670 (2017).

[14] Y. Arita, A. W. McKinley, M. Mazilu, H. Rubinsztein-Dunlop, and K. Dholakia, Picoliter rheology of gaseous media using a rotating optically trapped birefringent microparticle, Anal. Chem. **83**, 8855 (2011).

[15] Y. B. Jin, J. W. Yan, S. J. Rahman, J. Li, X. D. Yu, and J. Zhang, 6 GHz hyperfast rotation of an optically levitated nanoparticle in vacuum, Photon. Res. **9**, 1344 (2021).

[16] R. Reimann, M. Doderer, E. Hebestreit, R. Diehl, M. Frimmer, D. Windey, F. Tebbenjohanns, and L. Novotny, GHz rotation of an optically trapped nanoparticle in vacuum, Phys. Rev. Lett. **121**, 033602 (2018).

[17] J. Ahn, Z. Xu, J. Bang, Y. H. Deng, T. M. Hoang, Q. Han, R. M. Ma, and T. Li, Optically levitated nanodumbbell Torsion balance and GHz nanomechanical rotor, Phys. Rev. Lett. **121**, 033603 (2018).

[18] R. Zhao, A. Manjavacas, F. J. García de Abajo, and J. B. Pendry, Rotational quantum friction, Phys. Rev. Lett. **109**, 123604 (2012).

[19] A. Manjavacas and F. J. García de Abajo, Vacuum friction in rotating particles, Phys. Rev. Lett. **105**, 113601 (2010).

[20] Z. Xu and T. Li, Detecting casimir torque with an optically levitated nanorod, Phys. Rev. A **96**, 033843 (2017).

[21] A. Manjavacas, F. J. Rodríguez-Fortuño, F. J. García de Abajo, and A. V. Zayats, Lateral casimir force on a rotating particle near a planar surface, Phys. Rev. Lett. **118**, 133605 (2017).

[22] B. A. Stickler, K. Hornberger, and M. S. Kim, Quantum rotations of nanoparticles, Nature Rev. Phys. **3**, 589 (2021).

[23] B. A. Stickler, B. Papendell, and K. Hornberger, Spatio-orientational decoherence of nanoparticles, Phys. Rev. A **94**, 033828 (2016).

[24] B. Schrinski, B. A. Stickler, and K. Hornberger, Collapse-induced orientational localization of rigid rotors, J. Opt. Soc. Am. B **34**, C1 (2017).

[25] Y. Arita, M. Mazilu, and K. Dholakia, Laser-induced rotation and cooling of a trapped microgyroscope in vacuum, Nature Commun. **4**, 2374 (2013).

[26] A. D. Rider, C. P. Blakemore, A. Kawasaki, N. Priel, S. Roy, and G. Gratta, Electrically driven, optically levitated microscopic rotors, Phys. Rev. A **99**, 041802(R) (2019).

[27] M. Rashid, M. Toros, A. Setter, and H. Ulbricht, Precession motion in levitated optomechanics, Phys. Rev. Lett. **121**, 253601 (2018).

[28] Y. Arita, S. H. Simpson, P. Zemánek, and K. Dholakia, Coherent oscillations of a levitated birefringent microsphere in vacuum driven by nonconservative rotation-translation coupling, Sci. Adv. **6**, eaaz9858 (2020).

[29] J. Bang, T. Seberson, J. Ahn, P. Ju, Z. Xu, X. Gao, F. Robicheaux, and T. Li, Five-dimensional cooling and nonlinear

dynamics of an optically levitated nanodumbbell, Phys. Rev. Res. **2**, 043054 (2020).

[30] B. Max and W. Emil, *Principles of Optics* (Cambridge University Press, Cambridge, 1999).

[31] S. Xie, A. Sharma, M. Romodina, N. Y. Joly, and P. S. J. Russell, Tumbling and anomalous alignment of optically levitated anisotropic microparticles in Chiral hollow-core photonic crystal fiber, Sci. Adv. **7**, abf6053 (2021).

[32] A. Jonghoon, *Spin Optomechanics of Levitated Nanoparticles* (Purdue University, Indiana, 2020).

[33] F. Monteiro, S. Ghosh, E. C. van Assendelft, and D. C. Moore, Optical rotation of levitated spheres in high vacuum, Phys. Rev. A **97**, 051802(R) (2018).

[34] M. Li, S. Yan, B. Yao, Y. Liang, G. Han, and P. Zhang, Optical trapping force and torque on spheroidal Rayleigh particles with arbitrary spatial orientations, J. Opt. Soc. Am. A **33**, 1341 (2016).

[35] F. Monteiro, S. Ghosh, A. G. Fine, and D. C. Moore, Optical levitation of 10-ng spheres with nano-g acceleration sensitivity, Phys. Rev. A **96**, 063841 (2017).

[36] Y. Zheng, L.-M. Zhou, Y. Dong, C.-W. Qiu, X.-D. Chen, G.-C. Guo, and F.-W. Sun, Robust optical-levitation-based metrology of nanoparticle's position and mass, Phys. Rev. Lett. **124**, 223603 (2020).

[37] T. Delord, P. Huillery, L. Nicolas, and G. Hétet, Spin-cooling of the motion of a trapped diamond, Nature (London) **580**, 56 (2020).

[38] B. A. Stickler, B. Papendell, S. Kuhn, B. Schrinski, J. Millen, M. Arndt, and K. Hornberger, Probing macroscopic quantum superpositions with nanorotors, New J. Phys. **20**, 122001 (2018).

[39] P. Nagornykh, J. E. Coppock, J. P. J. Murphy, and B. E. Kane, Optical and magnetic measurements of gyroscopically stabilized graphene nanoplatelets levitated in an ion trap, Phys. Rev. B **96**, 035402 (2017).